Naval Research Laboratory

Washington, DC 20375-5320

NRL/MR/6703--14-9548

Remote Atmospheric Nonlinear Optical Magnetometry

PHILLIP SPRANGLE

Directed Energy Physics
Plasma Physics Division

LUKE JOHNSON

University of Maryland
College Park, Maryland

BAHMAN HAFIZI
ANTONIO TING

Beam Physics Branch
Plasma Physics Division

April 28, 2014

REPORT DOCUMENTATION PAGE

Form Approved
OMB No. 0704-0188

1. REPORT DATE *(DD-MM-YYYY)*	2. REPORT TYPE	3. DATES COVERED *(From - To)*
28-04-2014	Interim	September 2013 – April 2014

4. TITLE AND SUBTITLE

Remote Atmospheric Nonlinear Optical Magnetometry

5a. CONTRACT NUMBER

5b. GRANT NUMBER

5c. PROGRAM ELEMENT NUMBER

6. AUTHOR(S)

Phillip Sprangle, Luke Johnson,[1] Bahman Hafizi, and Antonio Ting

5d. PROJECT NUMBER
67-4660-04

5e. TASK NUMBER

5f. WORK UNIT NUMBER

7. PERFORMING ORGANIZATION NAME(S) AND ADDRESS(ES)

Naval Research Laboratory
4555 Overlook Avenue, SW
Washington, DC 20375-5320

8. PERFORMING ORGANIZATION REPORT NUMBER

NRL/MR/6703--14-9548

9. SPONSORING / MONITORING AGENCY NAME(S) AND ADDRESS(ES)

Naval Research Laboratory
4555 Overlook Avenue, SW
Washington, DC 20375-5320

10. SPONSOR / MONITOR'S ACRONYM(S)

NRL

11. SPONSOR / MONITOR'S REPORT NUMBER(S)

12. DISTRIBUTION / AVAILABILITY STATEMENT

Approved for public release; distribution is unlimited.

13. SUPPLEMENTARY NOTES

[1]University of Maryland, College Park, MD 20742-4111

14. ABSTRACT

In this paper an analysis of remote atmospheric magnetometry concepts, based on using molecular oxygen as the paramagnetic species, is presented. The objective is to use these concepts as possible mechanisms for the detection of underwater and underground objects. The formulation is based on the coupled Maxwell-density matrix system of equations. We use these coupled equations to describe the magnetization of a paramagnetic species in the presence of an intense modulated laser pulse and ambient magnetic field. The O_2 magnetic dipole transition line that is considered is the $b^1\Sigma_g^+ - X^3\Sigma_g^-$ transition band of oxygen near 762 nm. A high-intensity, repetition rate, polarized titanium-doped sapphire laser is considered for the pump. The nonlinear formulation is used to investigate magnetic anomaly detection mechanisms using i) wakefield polarization rotation and, ii) polarization changes in resonance fluorescence emission (Hanle effect). The major challenges for these related approaches is the collisional dephasing of the atmospheric oxygen transitions and the strength of the magnetic dipole moment.

15. SUBJECT TERMS

Remote atmospheric magnetometry
Magnetometry
Nonlinear optical
Oxygen molecule

16. SECURITY CLASSIFICATION OF:			17. LIMITATION OF ABSTRACT	18. NUMBER OF PAGES	19a. NAME OF RESPONSIBLE PERSON
a. REPORT	b. ABSTRACT	c. THIS PAGE			Phillip Sprangle
Unclassified Unlimited	Unclassified Unlimited	Unclassified Unlimited	Unclassified Unlimited	20	19b. TELEPHONE NUMBER *(include area code)* (202) 767-3493

Standard Form 298 (Rev. 8-98)
Prescribed by ANSI Std. Z39.18

Remote Atmospheric Nonlinear Optical Magnetometry

Phillip Sprangle, Luke Johnson[1], Bahman Hafizi and Antonio Ting

Plasma Physics Division, Naval Research Laboratory, Washington DC 20375

[1]University of Maryland, College Park, Maryland 20742-4111

Abstract

In this paper an analysis of remote atmospheric magnetometry concepts, using molecular oxygen as the paramagnetic species is considered. The objective is to use these mechanisms for the remote detection of underwater and underground objects. We use the coupled Maxwell-density matrix system of equations to describe the magnetization of the paramagnetic species in the presence of an intense modulated laser pulse and ambient magnetic field. The magnetic dipole transition line that is considered is the $b^1\Sigma_g^+ - X^3\Sigma_g^-$ transition band of O_2 near 762 nm. The pump is taken to be a high-intensity, pulsed, polarized titanium-doped sapphire laser. The model is used to investigate a magnetic anomaly detection signature using the polarization rotation of the wakefield behind the pump pulse. The major challenges are the collisional dephasing of the atmospheric oxygen transitions and the strength of the effective magnetic dipole interaction.

Manuscript Approved April 11, 2014

I. Introduction

Optical magnetometry is a highly sensitive method for measuring small variations in magnetic fields [1-3]. The development of a remote optical magnetometry system would have important applications for the detection of underwater and underground objects that perturb the local ambient magnetic field. In our remote atmospheric optical magnetometry model, a high-intensity laser pulse is employed to drive the magnetic spin precession in the presence of the earth's magnetic field. Zeeman splitting of the molecular energy levels and consequently the precessional frequency are proportional to the local magnetic field. This can, in principle, provide a precise means to measure variations in the Earth's magnetic field. For a number of magnetic anomaly detection (MAD) applications, μG magnetic field variations must be detected at standoff distances of approximately one kilometer from the sensor [4].

In this paper we consider atmospheric molecular oxygen as the paramagnetic species in a nonlinear remote optical magnetometry configuration depicted Fig. 1. The propagation of the high-intensity pump laser pulse to remote (~ km) detection sites is considered. By employing the optical Kerr effect we show that high laser intensities (10^{12} W/cm^2) can be propagated to remote locations. Using a high-intensity polarized laser pulse we consider the polarization rotation of the wakefield behind the pump pulse. The pump intensity is limited (< 10^{12} W/cm^2) to avoid photoionization processes.

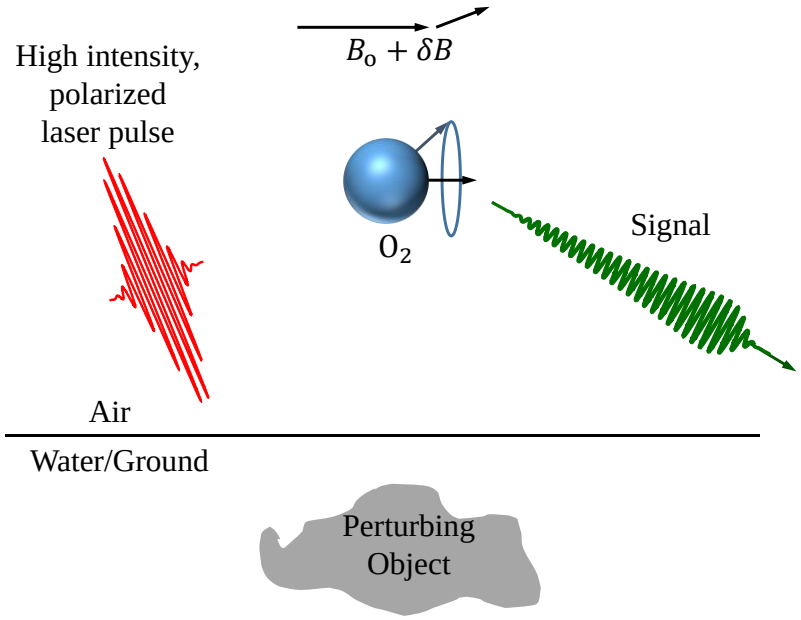

Figure 1: Remote nonlinear optical magnetometry configuration. The Earth's magnetic field is $B_o \approx 0.5\text{G}$ and δB is the perturbation caused by the underwater/underground object.

Molecular oxygen's paramagnetic response is due to two unpaired valance electrons. The ground state of oxygen $X^3\Sigma_g^-$, commonly referred to as "triplet oxygen," has total angular

momentum $J=1$, total spin $S=1$ and three degenerate sublevels. The excited upper state being considered is denoted by $b^1\Sigma_g^+$. It has $J=0$ and is a spin singlet $S=0$ state with only one sublevel. The upper state can undergo three radiative transitions, $b^1\Sigma_g^+ \rightarrow X^3\Sigma_g^-(m=\pm 1)$, $b^1\Sigma_g^+ \rightarrow X^3\Sigma_g^-(m=0)$, but the latter is insignificant because it is an electric quadruple transition. There is an intermediate state, referred to as $a^1\Delta_g$, into which the excited O_2 molecule can decay and is discussed in Appendix A. The O_2 transition line being considered is the $b^1\Sigma_g^+ - X^3\Sigma_g^-$ transition band of oxygen near 762 nm. In the low laser intensity, long pulse, regime this transition has been investigated theoretically [5,6] and experimentally [7] and is a prominent feature of air glow.

In this paper, a high intensity, polarized titanium-doped sapphire laser is considered for the pump laser. These lasers have an extremely large tuning range from 660 nm to 1180 nm, and can have linewidths that are transform limited. A major challenge for this, as well as any remote atmospheric optical magnetometry concept, is collisional dephasing (elastic collisions) of the transitions. The elastic molecular collision frequency, at standard temperature and pressure (STP), is $\gamma_c = N_{\text{air}}\sigma v_{th} = 3.5\times 10^9\,\text{sec}^{-1}$, where σ is the molecular cross section and v_{th} is the thermal velocity [7]. On the other hand, the Larmor frequency (spin precession) in the Earth's magnetic field, $B_o \approx 0.5\text{G}$, is $\Omega_o = qB_o/(2mc) \approx 4.5\times 10^6\,\text{rad/sec}$ ($\hbar\Omega_o = 3\times 10^{-9}\,\text{eV}$), where m and q are the electron mass and charge and c is the speed of light. Since the dephasing frequency is far greater than the Larmor frequency, the parameters are somewhat restrictive for remote atmospheric magnetometry. However, rotational magnetometry experiments based on molecular oxygen at STP and magnetic fields of ~ 10 G have shown measurable linear Faraday rotational effects [7].

II. Atmospheric Propagation of Intense Laser Pulses (Focusing & Compression)

The magnetic anomaly detection concepts considered here rely on propagation of intense laser beams in the atmosphere. Atmospheric propagation of intense, short pulse lasers are strongly affected by various interrelated linear and nonlinear processes [8]. These include diffraction, Kerr focusing, group velocity dispersion, spectral broadening and self-phase modulation. Pulse compression can be achieved by introducing a frequency chirp on the pulse; however, for the problem under consideration, pulse compression is not significant. Nonlinear transverse focusing results from the Kerr effect. In general, a laser pulse propagating in air can be longitudinally and transversely focused at remote distances (> km) to reach high intensities (~10^{12} W/cm^2), as indicated in Fig. 2.

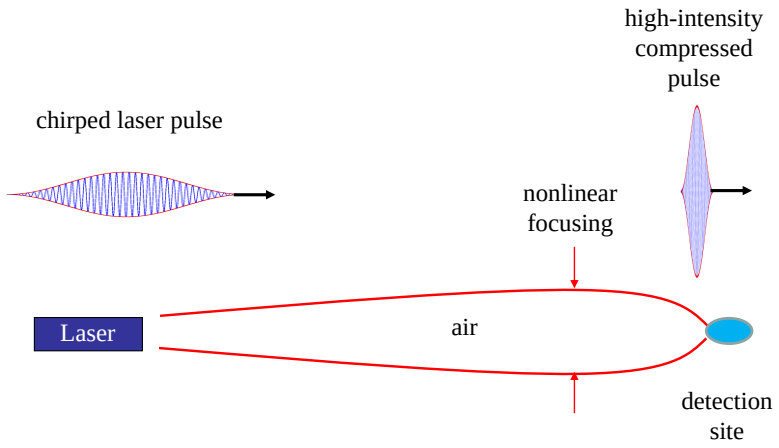

Figure 2: Simultaneous transverse focusing and longitudinal compression of a chirped laser pulse in air due to nonlinear self-focusing and group velocity dispersion.

Here we present the model describing longitudinal and transverse compression of a chirped laser pulses in air [8]. For optimally chosen parameters, the longitudinal and transverse focal distances can be made to coincide resulting in a rapid intensity increase near the focal region.

The laser electric field is given by $\mathbf{E}(r,\eta,\tau)=(1/2)\hat{E}(r,\eta,\tau)e^{-i\omega\tau}\,\hat{\mathbf{e}}_x+\text{c.c.}$, where $\hat{E}$ is the complex amplitude, ω is the frequency, r is the radial coordinate, $\tau=t-z/c$ and $\eta=z$ are the transformed coordinates, the propagation distance z and time t are in the laboratory frame. Substituting this field representation into the wave equation results in a higher order paraxial wave equation for $\hat{E}(r,\eta,\tau)$ [8],

$$\left[\nabla_\perp^2+2ik\frac{\partial}{\partial\eta}-c^2k\beta_2\frac{\partial^2}{\partial c^2\tau^2}+\frac{\omega^2 n_K}{4\pi c}\left|\hat{E}(r,\eta,\tau)\right|^2\right]\hat{E}(r,\eta,\tau)=0, \qquad (1)$$

where the wavenumber is $k=\omega/c$ and the group velocity dispersion parameter is $\beta_2=2.2\times10^{-31}\text{sec}^2/\text{cm}$. The nonlinear refractive index of air is $n=1+n_K I$, where the Kerr nonlinear index is $n_K=3\times10^{-19}\text{cm}^2/\text{W}$ and I is the laser intensity. The values for β_2 and n_K apply to air at STP and $\lambda=2\pi/k\approx762\,\text{nm}$.

Equation (1) can be solved by assuming the pulse is described by a form that depends on certain spatially-dependent parameters. With this assumption, a set of simplified coupled equations can be derived for the evolution of the spot size, pulse duration, amplitude and phase of the laser field. Taking the laser pulse to have a Gaussian shape in both the transverse and longitudinal directions, the complex amplitude can be written as

$$\hat{E}(r,\eta,\tau)=E_o(\eta)e^{i\theta(\eta)}e^{-(1+i\alpha(\eta))r^2/R^2(\eta)}e^{-(1+i\beta(\eta))\tau^2/T^2(\eta)}, \qquad (2)$$

where $E_o(\eta)$ is the field amplitude, $\theta(\eta)$ is the phase, $R(\eta)$ is the spot size, $\alpha(\eta)$ is related to the curvature of the wavefront, $T(\eta)$ is the laser pulse duration, and $\beta(\eta)$ is the chirp parameter. The quantities E_o, θ, T, R, α, β are real functions of the propagation distance η. The instantaneous frequency spread along the pulse, i.e., chirp, is $\delta\omega(\eta,\tau) = 2\beta(\eta)\tau / T^2(\eta)$, where $\beta(\eta) = T(\eta)/(2\beta_2)\partial T(\eta)/\partial\eta < 0 (> 0)$ results in a negative (positive) frequency chirp, i.e., frequency decreases (increases) towards the back of the pulse.

Substituting Eq. (2) into Eq. (1) and equating like powers of r and τ, the following coupled equations for R and T are obtained,

$$\frac{\partial^2 R}{\partial \eta^2} = \frac{4}{k^2 R^3}\left(1 - \frac{\mathcal{E}_o}{P_{NL}}\frac{1}{T}\right), \tag{3a}$$

$$\frac{\partial^2 T}{\partial \eta^2} = \frac{4\beta_2}{k}\frac{\mathcal{E}_o}{P_{NL}}\frac{1}{R^2 T^2} + \frac{4\beta_2^2}{T^3}, \tag{3b}$$

where $\mathcal{E}_o = P(0)T(0)$ is proportional to the laser pulse energy and is independent of η, $P(\eta) = \pi R^2(\eta) I(\eta)/2$ is the laser power, $I(\eta) = cE_o^2(\eta)/(8\pi) = I(0)R^2(0)T(0)/(R^2(\eta)T(\eta))$ is the peak intensity and $P_{NL} = \lambda^2/(2\pi n_K)$ is the self-focusing power. In Eq. (3) the initial conditions are given by $\alpha(0) = -(kR(0)/2)\partial R(0)/\partial\eta$ and $\beta(0) = T(0)/(2\beta_2)\partial T(0)/\partial\eta = 0$. The first term on the right hand side of Eq. (3a) describes vacuum diffraction while the second term describes nonlinear self-focusing, i.e., due to n_K. Nonlinear self-focusing dominates diffraction resulting in filamentation when $P > P_{NL} \approx 3\text{GW}$ [8,9].

In the limit that the pulse length does not change appreciably the laser spot size is given by $R(\eta) = R(0)\left[1 - 2\alpha(0)\eta/Z_{R0} + (1 - P/P_{NL} + \alpha^2(0))(\eta/Z_{R0})^2\right]^{1/2}$, where $Z_{R0} = kR^2(0)/2$ is the Rayleigh length. The spot size reaches a focus in a distance $\eta/Z_{R0} = \alpha(0)/\left(1 - P/P_{NL} + \alpha^2(0)\right)$ as long as $P < (1 + \alpha^2(0))P_{NL}$.

Figures 3(a) and 3(b) show the evolution of the laser spot size and the intensity as a function of propagation distance for $\lambda = 762\,\text{nm}$. At focus, the laser intensity ($I_{\text{focus}} = 6\times10^{10}\,\text{W/cm}^2$) and spot size ($R_{\text{focus}} = 1.3\,\text{mm}$) are held constant by choosing appropriate initial conditions: wavefront curvature $\alpha(0) = 37$, pulse duration $T(0) = 100\,\text{psec}$, and chirp $\beta(0) = 0$. By changing the laser energy and the initial spot size, the nonlinear self-focusing effect changes the focal point from 0.25 km to 0.75 km (see Fig. 3). Nonlinear laser pulse propagation allows for moving of the detection site location.

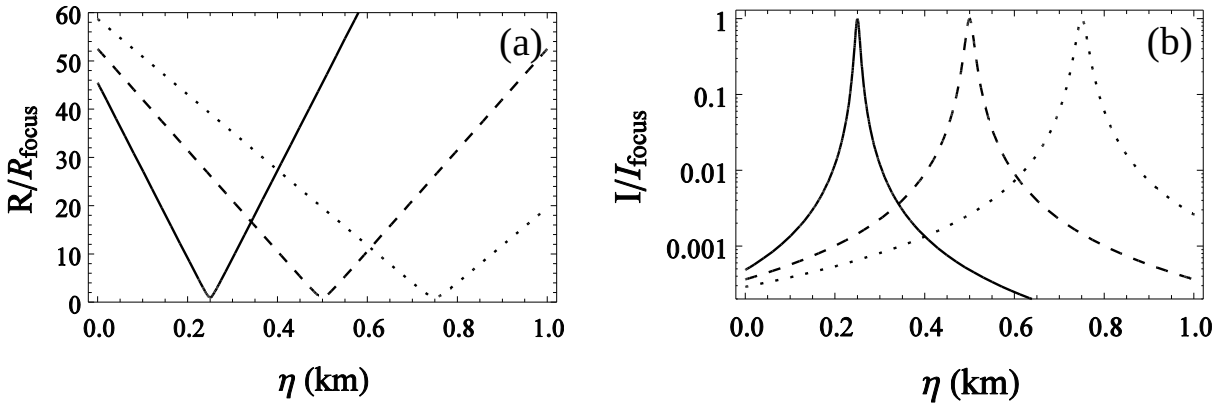

Figure 3: Evolution of (a) laser spot size and (b) normalized peak laser intensity as functions of propagation distance for different initial laser energies and spot sizes. The laser energy and initial spot size for the solid, dashed, and dotted lines are $\mathcal{E}_o = 100, 150, 190$ mJ and $R(0) = 4.7, 6.7, 8.2$ cm, respectively.

III. Optical Magnetometry Model

The four levels of O_2 being considered in the magnetometry model are shown in Fig. 4. The ground state is split by the Zeeman effect into three levels $|1\rangle$, $|2\rangle$, and $|3\rangle$ and the excited state is denoted by $|4\rangle$. The magnetic quantum number *m* associated with the various levels is indicated in Fig. 4. The excited state, level $|4\rangle$, can be populated by right hand polarized (RHP) light from level $|3\rangle$ or by left hand polarized light (LHP) light from level $|1\rangle$. Here the quantization axis and the direction of the static magnetic field are taken to be along the direction of laser propagation, z – axis. Circularly polarized radiation carries angular momentum $\pm\hbar$ which is directed along the propagation direction, hence the selection rule for allowed transitions is $\Delta m = \pm 1$, which will conserve angular momentum [10]. It should be noted that this transition is strictly magnetic dipole- and spin-forbidden, but spin-orbit coupling between the $b^1\Sigma_g^+$ and $X^3\Sigma_g^-(m=0)$ states leads to a transition with a magnetic dipole-like nature and a larger than expected dipole moment [5,6,11].

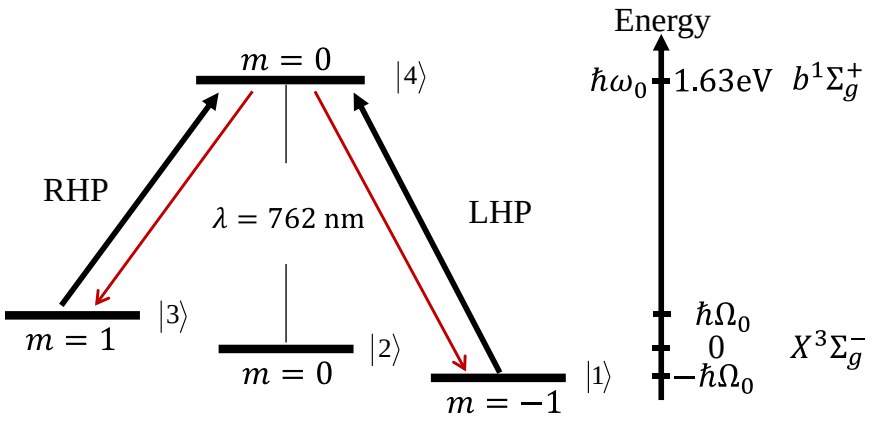

Figure 4: Energy levels associated with the ground and excited state of O_2. The transition frequency corresponds to ~ 762 nm ($\hbar\omega_A = 1.63\text{eV}$). The Zeeman splitting of the ground state is caused by the ambient magnetic field.

A high-intensity pump pulse generates a magnetization current density $\mathbf{J}_M = c\nabla\times\mathbf{M}$, where $\mathbf{M}$ is the magnetization field. The current density in turn generates a response electric field and can also modify the pump pulse. The response electric field $\mathbf{E}$ is given by (Gaussian units) $\left(\nabla^2 - (1/c^2)\partial^2/\partial t^2\right)\boldsymbol{E} = (4\pi/c^2)\partial\boldsymbol{J}_M/\partial t = (4\pi/c)\partial(\nabla\times\boldsymbol{M})/\partial t$. The magnetization is represented by a sum of RHP and LHP components $\mathbf{M}(z,t) = M_R(z,t)\hat{\mathbf{e}}_R + M_L(z,t)\hat{\mathbf{e}}_L + \text{c.c.}$, where $M_R(z,t) = N\mu_m\rho_{43}(z,t)$, $M_L(z,t) = N\mu_m\rho_{41}(z,t)$, N is the density of the paramagnetic species (oxygen molecules), μ_m is the effective magnetic dipole moment associated with the transitions, ρ_{43} and ρ_{41} are the off-diagonal coherence of the allowed density matrix elements (see Fig. 4) and $\hat{\mathbf{e}}_{R,L} = (\hat{\mathbf{e}}_x \pm i\hat{\mathbf{e}}_y)/2$ are vectors denoting the polarization direction. The magnetization current density can be written as $\boldsymbol{J}_M = -ic\partial M_R(z,t)/\partial z\hat{\mathbf{e}}_R +$ $ic\partial M_L(z,t)/\partial z\hat{\mathbf{e}}_L + \text{c.c.}$ In terms of the x and y components,

$$\mathbf{J}_M = -i(c/2)\partial(M_R - M_L)/\partial z\hat{\mathbf{e}}_x + i(c/2)\partial(M_R + M_L)/\partial z\hat{\mathbf{e}}_y + \text{c.c.}$$

The density matrix equation is given by [10,12,13] $\partial\rho_{nm}/\partial t = -i\omega_{nm}\rho_{nm} +$ $i\sum_\ell\{\Omega_{nl}\rho_{lm} - \Omega_{lm}\rho_{ln}\} + \text{relaxation terms}$, where $\omega_{nm} = \omega_n - \omega_m$, Ω_{nm} denotes the interaction frequency, the phenomenological relaxation terms are due to elastic and inelastic collisions, and spontaneous transitions and the magnetic dipole interaction Hamiltonian is $-\boldsymbol{\mu}_m\cdot\mathbf{B}$ (Appendix B). The off-diagonal coherence elements of the density matrix for the relevant transitions ($|1\rangle\rightarrow|4\rangle$ and $|3\rangle\rightarrow|4\rangle$) are given by

$$\partial\rho_{41}/\partial t = -\gamma_c\rho_{41} - i\omega_{41}\rho_{41} + i\Omega_{41}\left(\rho_{11}-\rho_{44}\right) + i\Omega_{43}\rho_{31}, \tag{4a}$$

$$\partial\rho_{43}/\partial t = -\gamma_c\rho_{43} - i\omega_{43}\rho_{43} + i\Omega_{43}\left(\rho_{33}-\rho_{44}\right) + i\Omega_{41}\rho_{13}, \tag{4b}$$

where γ_c is the elastic collision frequency (not population transferring), the full set of density matrix equations are given in Appendix B.

The pump laser field, which induces the magnetization field, is expressed as a sum of RHP and LHP fields $\mathbf{B}_{\text{pump}}(z,t) = B_R(z,t)\hat{\mathbf{e}}_R + B_L(z,t)\hat{\mathbf{e}}_L + \text{c.c.}$, where $B_{R,L}(z,t) = \hat{B}_{R,L}(z,t)e^{i\psi(z,t)}$ and $\psi(z,t) = kz - \omega t$. The interaction frequencies associated with the allowed transitions are $\Omega_{43} = \mu_m B_R(z,t)/\hbar = \hat{\Omega}_R(z,t)e^{i\psi(z,t)}$ and $\Omega_{41} = \mu_m B_L(z,t)/\hbar = \hat{\Omega}_L(z,t)e^{i\psi(z,t)}$, where $\hat{\Omega}_{R,L} = \mu_m \hat{B}_{R,L}/\hbar$ is (half) the Rabi frequency associated with the RHP and LHP components of the pump. Note that the Rabi frequency is defined with respect to the peak field.

Although we are considering a magnetic dipole transition it is convenient to express the Rabi frequency normalized to an electric dipole moment. The magnitude of the Rabi frequency can be written as $\hat{\Omega}_{\text{Rabi}} = \mu_m \hat{B}_{\text{peak}}/\hbar = (\mu_m/\mu_e)(\mu_e \hat{E}_{\text{peak}}/\hbar) = (\mu_m/\mu_e)(\mu_e/\hbar)(8\pi I/c)^{1/2}$, where $I = c\hat{E}_{\text{peak}}^2/(8\pi)$ is the pump laser intensity and $\hat{E}_{\text{peak}}$ is the peak field. Taking the normalizing electric dipole moment to be $\mu_e = q r_B = 2.5\times10^{-18}$ statC-cm, where r_B is the Bohr radius the magnitude of the Rabi frequency is $\hat{\Omega}_{\text{Rabi}}[\text{rad/sec}] = 2.5\times10^8\ (\mu_m/\mu_e)\sqrt{I[\text{W/cm}^2]}$. As an example, for $I = 10^{11}\ \text{W/cm}^2$ and $\mu_m/\mu_e = 10^{-4}$, the Rabi frequency is $\hat{\Omega}_{\text{Rabi}} = 8\times10^9$ rad/sec.

IV. Faraday Rotation of Wakefields Driven by Intense Laser Pulses

The incident pump field is taken to be polarized in the x-direction $\mathbf{E} = \hat{E}_o(z,t)e^{-i(kz-\omega t)}\left(\hat{\mathbf{e}}_R + \hat{\mathbf{e}}_L\right) + \text{c.c.}$, where ω is the carrier laser frequency and the complex pulse amplitude $\hat{E}_o(z,t)$ can be modulated. Employing the variables $\tau = t - z/c$ and $\eta = z$, $\mathbf{E} = \hat{E}_o(\tau)e^{-i\omega\tau}e^{i\Delta k\eta}(\hat{\mathbf{e}}_R + \hat{\mathbf{e}}_L) + \text{c.c.}$, the corresponding magnetic field in the y-direction is $\mathbf{B} = -i\hat{E}_o(\tau)e^{-i\omega\tau}e^{i\Delta k\eta}(\hat{\mathbf{e}}_R - \hat{\mathbf{e}}_L) + \text{c.c.}$, where $\Delta k = k - \omega/c \approx 2\pi i kN\mu_m^2\rho_{11}/(\hbar\gamma_c)$ is the wavenumber mismatch (damping) obtained from the linear dispersion relation. The characteristic wavenumber mismatch for $\lambda = 762\,\text{nm}$ at atmospheric molecular oxygen density $N = 5.7\times10^{18}\,\text{cm}^{-3}$ and an equilibrium population of $\rho_{11} = 1/3$ is $i\Delta k = -\Gamma_D = -1.7\times10^{-3}\,\text{cm}^{-1}$ $\left(1/\Gamma_D \approx 6\,\text{m}\right)$. As the pulse propagates through the atmosphere it induces a magnetization current which generates a field polarized in both the x and y directions. The wave equation for the forward propagating, y-component of the complex field amplitude is

$(\partial/\partial\eta + i\Delta k)\hat{E}_y(\eta,\tau) = -i\,2\pi N\mu_m k\left(\hat{\rho}_{43}(\tau)+\hat{\rho}_{41}(\tau)\right)$, where the Faraday rotated field is $\hat{E}_y(\eta,\tau)e^{-i\omega\tau}\,e^{i\Delta k\eta}\,\hat{\mathbf{e}}_y + c.c.$ The magnetization current is a function of the off-diagonal coherence terms of the density matrix elements $\rho_{43}(\eta,\tau)=\hat{\rho}_{43}(\tau)e^{-i\omega\tau}\,e^{i\Delta k\eta}$ and $\rho_{41}(\eta,\tau)=\hat{\rho}_{41}(\tau)e^{-i\omega\tau}\,e^{i\Delta k\eta}$. The slowly varying quantities $\hat{\rho}_{43}(\tau)$ and $\hat{\rho}_{41}(\tau)$ are given by reduced density matrix equations $(\partial/\partial\tau - i\Delta\omega_{43})\hat{\rho}_{43}(\tau) = i\hat{\Omega}_{43}(\tau)\rho_o$ and $(\partial/\partial\tau - i\Delta\omega_{41})\hat{\rho}_{41}(\tau) = i\hat{\Omega}_{41}(\tau)\rho_o$, where $\hat{\Omega}_{43}(\tau) = -i\mu_m\hat{E}_o(\tau)/\hbar$, $\hat{\Omega}_{41} = i\mu_m\hat{E}_o(\tau)/\hbar$, $\rho_o = \rho_{11} = \rho_{22} = \rho_{33} = 1/3$, $\rho_{44} = 0$, $\Delta\omega_{nm} = \omega - \omega_{nm} + i\gamma_c$, $\omega_{43} = \omega_A - \Omega_o$, $\omega_{41} = \omega_A + \Omega_o$ and it has been assumed that $c|\Delta k|/\omega \ll 1$.

In the case where the pump amplitude is not modulated in amplitude or frequency, i.e., conventional Faraday rotation within a long pump duration, $\partial/\partial\tau = 0$, the spatial change in the Faraday rotated field is given by $(\partial/\partial\eta + i\Delta k)\hat{E}_y(\eta,\tau) = 2\pi kN\mu_m^2(\hat{E}_o/\hbar)\rho_o\Omega_o/\gamma_c^2$. After propagating a distance *L*, the ratio between the Faraday rotated and incident intensities is $I_y/I_o = |E_y|^2/|E_o|^2 = (2\pi)^4(L/\lambda)^2(N\mu_m^2\rho_o/\hbar)^2\,(\Omega_o/\gamma_c^2)^2$.

In the present model the pump pulse consists of a pulse train, as shown in Fig. 5, in which the duration of the individual micropulses, denoted by τ_p, can be comparable or longer than the damping time $1/\gamma_c$. However, the time separation between the micropulses T is taken to be long compared to a damping time. With this ordering of timescales the individual pump pulses excite the density matrix elements ρ_{43} and ρ_{41} which generate a wakefield that decays behind the individual pump pulses (Fig. 5). The magnetization currents generate a Faraday rotated wakefield behind each pump pulse.

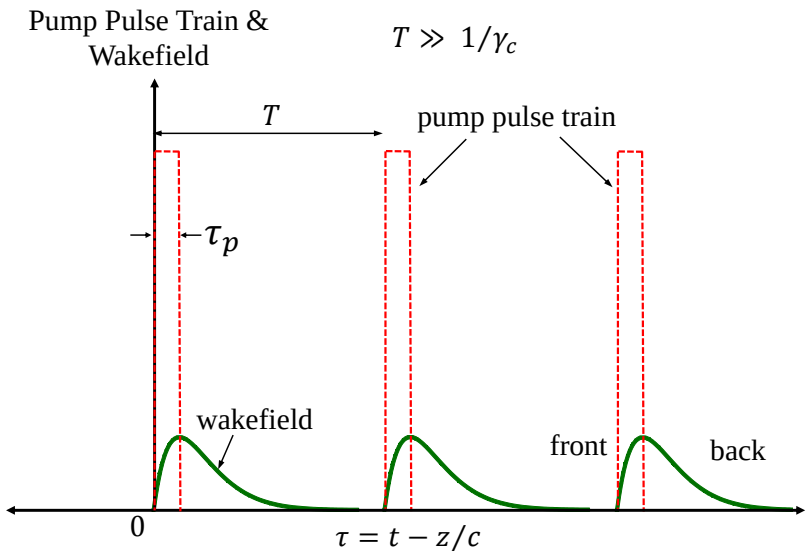

Figure 5: Pump pulse train and induced polarization rotated wakefields.

The general form of the off-diagonal coherence elements is

$(\partial/\partial\tau - i\Delta\omega_{nm})\hat{\rho}_{nm}(\tau) = i\hat{\Omega}_{nm}(\tau)\rho_o$ with solution $\hat{\rho}_{nm}(\tau) = i\rho_o\int_0^\tau d\tau'\,\hat{\Omega}_{nm}(\tau')\exp(-i\Delta\omega_{nm}(\tau'-\tau))$

within the pump pulse. The solution behind the pump pulse is $\hat{\rho}_{43}(\tau) = \hat{\rho}_{43}(\tau_p)\exp(i\Delta\omega_{43}(\tau-\tau_p))$ and $\hat{\rho}_{41}(\tau) = \hat{\rho}_{41}(\tau_p)\exp(i\Delta\omega_{41}(\tau-\tau_p))$. The reduced wave equations for the x and y components of the wakefields are

$$(\partial/\partial\eta + i\Delta k)\hat{E}_x(\eta,\tau) = -(2\pi/c)\,\hat{J}_{Mx}(\tau) = -C_o k\rho_o W_x(\tau)\hat{E}_o, \tag{5a}$$

$$(\partial/\partial\eta + i\Delta k)\hat{E}_y(\eta,\tau) = -(2\pi/c)\,\hat{J}_{My}(\tau) = iC_o k\rho_o W_y(\tau)\hat{E}_o, \tag{5b}$$

where $k = \omega/c$, $\omega >> |\partial/\partial\tau|$, $c|\Delta k|$ and $C_o = 2\pi(N\mu_m^2/\hbar)/\gamma_c \approx 6\times10^{-7}$ is a unitless parameter. In estimating C_o we have taken the magnetic dipole moment to equal $\mu_m = \mu_e\times10^{-4} = 2.5\times10^{-22}$ statC-cm, the collision frequency to be $\gamma_c = 3.5\times10^9\ \text{sec}^{-1}$ and the O_2 density to be $N = 5.7\times10^{18}\,\text{cm}^{-3}$. The current densities are $\hat{J}_{Mx}(\tau) = (N\mu_m\omega/2)(\hat{\rho}_{43}(\tau) - \hat{\rho}_{41}(\tau))$ and $\hat{J}_{My}(\tau) = -(N\mu_m\omega/2)(\hat{\rho}_{43}(\tau) + \hat{\rho}_{41}(\tau))$, behind the pulse ($\tau \geq \tau_p$) they are given by

$$\hat{J}_{Mx}(\tau) = \frac{N\mu_m^2\hat{E}_o\rho_o}{\hbar}\frac{\omega\gamma_c}{\Omega_o^2+\gamma_c^2}W_x(\tau), \tag{6a}$$

$$\hat{J}_{My}(\tau) = -i\frac{N\mu_m^2\hat{E}_o\rho_o}{\hbar}\frac{\omega\gamma_c}{\Omega_o^2+\gamma_c^2}W_y(\tau), \tag{6b}$$

where the time dependence of the wakefield is captured by

$$W_x(\tau) = e^{-\gamma_c(\tau-\tau_p)}\Big[\cos(\Omega_o(\tau-\tau_p)) - e^{-\gamma_c\tau_p}\cos(\Omega_o\tau) - (\Omega_o/\gamma_c)\Big(\sin(\Omega_o(\tau-\tau_p)) - e^{-\gamma_c\tau_p}\sin(\Omega_o\tau)\Big)\Big], \tag{7a}$$

$$W_y(\tau) = e^{-\gamma_c(\tau-\tau_p)}\Big[\sin(\Omega_o(\tau-\tau_p)) - e^{-\gamma_c\tau_p}\sin(\Omega_o\tau) + (\Omega_o/\gamma_c)\Big(\cos(\Omega_o(\tau-\tau_p)) - e^{-\gamma_c\tau_p}\cos(\Omega_o\tau)\Big)\Big]. \tag{7b}$$

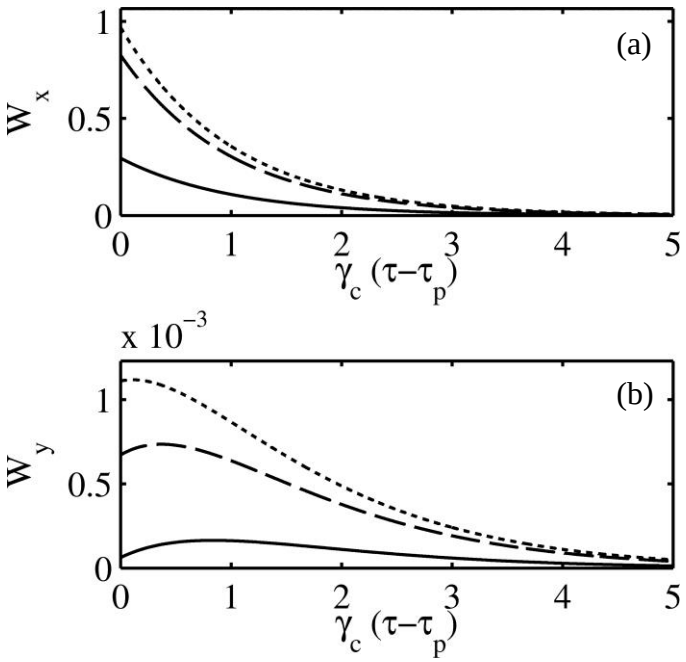

Figure 6: (a) x-component and (b) y-components of the wakefield response functions $W_{x,y}(\tau)$ behind the pulse for $\Omega_o = 4.5\times10^6$ rad/sec. The pulse durations for the solid, dashed, and dotted lines are $\tau_p = 0.1$ ns, 0.5 ns, 1 ns, respectively.

Figure 6 shows the wakefield time dependence, Eqs. (7), for pump pulse durations of $\tau_p =$ 0.1, 0.5, and 1 nsec, pump pulse energy of 100 mJ, and spot size of 1 mm. This results in a range of pump intensities from 6×10^9 W/cm^2 to 6×10^{10} W/cm^2. Equations (5) indicates that $\hat{E}_{x,y}/\hat{E}_0$ is proportional to $W_{x,y}(\tau)$, if Δk is neglected. For the parameters in Fig. 6, the normalized peak wakefield amplitudes are $\left|\hat{E}_x/\hat{E}_o\right| \approx 0.5$, 1.5, and 1.6 and $\left|\hat{E}_y/\hat{E}_o\right| \approx 1\times10^{-4}$, 1.2×10^{-3}, and 2×10^{-3}. There is a tradeoff between driving the wakefields with a higher

intensity pump ($\hat{E}_o \sim \tau_p^{-1/2}$) versus driving it for a longer duration ($W_{x,y} \sim \tau_p$). As a result, for $\tau_p > 3/\gamma_c$ the wakefield amplitude begins monotonically decreasing

For remote magnetic anomaly detection small spatial differences in the magnetic field must be measured. Here we consider measuring the differences in wakefield intensities at two nearby locations. The locations are referred to as (1) and (2) and have local magnetic fields B_o and $B_o + \delta B$. The intensity of the wakefield at location (1) and (2) is I_1 and I_2, respectively. The fractional change in intensity of the y-polarized wakefield is $|I_1 - I_2| / I_1 = |\delta I| / I_1 \approx 2\left|\delta \hat{E}_y / \hat{E}_{1y}\right|$, where $\hat{E}_{1y}$ is the y-component of the wakefield amplitude and $\delta \hat{E}_y$ is the difference in the wakefield amplitudes between the two locations. Figure 7 shows the fractional wakefield intensities for various values of δB. For the values shown, $|\delta I| / I_1 \sim 10^{-3}$.

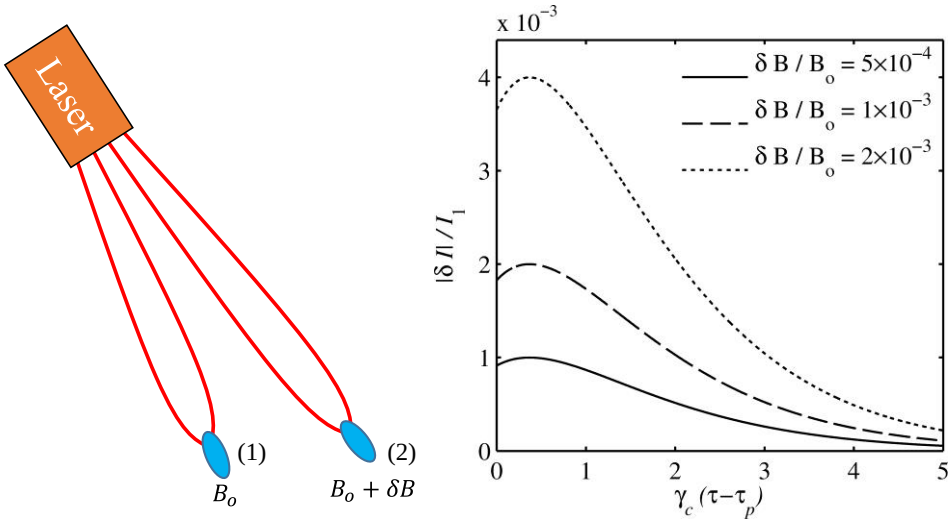

Figure 7: Fractional difference in the wakefield intensity for various fractional differences in the magnetic field $\delta B / B_o$. The pump pulse has duration $\tau_p = 500$ psec, spot size 1 mm, and energy 100 mJ. The differences in magnetic field and corresponding intensities are from two nearby locations.

The pump pulse energy is $I(\pi/2)R^2\tau_p$, where R is the spot size. For a pulse of duration $\tau_p = 500\,\text{psec} \approx 2/\gamma_c$, $R = 0.1\text{cm}$ and intensity $I = 10^{10}\,\text{W/cm}^2$, the pump pulse energy is $80\,\text{mJ/pulse}$. For a pulse train, rep-rated at $f_p = 1\text{kHz}$, the average pump laser power is $\langle P \rangle = f_p I(\pi/2)R^2\tau_p = 80\text{W}$.

It is worth noting that at sufficiently high intensities, the upper level, level $|4\rangle$, can be populated resulting in a laser induced florescence signal to lower energy levels, i.e. levels $|1\rangle$ and $|3\rangle$. This process is known as the Hanle effect and is briefly discussed in Appendix C. The magnetization current resulting from the induced florescence of an x polarized pump laser is $\mathbf{J}_M \propto e^{-\gamma_c \tau}\cos(\omega\tau)\left[\cos(\Omega_o\tau)\hat{\mathbf{e}}_x - \sin(\Omega_o\tau)\hat{\mathbf{e}}_y\right]$ [10]. Using polarization filters, the intensity on a detector due to the x and y components of the current density can be measured separately. Taking the ratio of the intensities from the x and y components of $\mathbf{J}_M$ gives $I_x/I_y \propto \cot^2(\Omega_o\tau)$. Note that the ratio is independent of the collision rate as long as the individual intensities are greater than the inherent intensity fluctuations.

V. Discussion and Concluding Remarks

Remote magnetometry has important applications, such as detection of underwater and underground objects. Detection of the magnetic anomaly caused by such an object is important to Navy missions. In the laboratory, under controlled environment, conventional magnetometry techniques can be used to measure extremely small magnetic field perturbations ($\sim \mu$G). Limitations on remote detection include collisional dephasing of magnetic fluctuations, air turbulence, etc.

The paramagnetic species considered here is the oxygen molecule which has the magnetic dipole transition ($b^1\Sigma_g^+ - X^3\Sigma_g^-$) near 762 nm. We considered an intense pump laser to induce a polarization rotation of the wakefield. This transition is resonantly driven by a linearly-polarized pump laser pulse. Our examples suggest that the intensity of the rotated component of the wakefield can be measured.

Numerous issues remain to be considered, these include signal-to-noise ratio limitations, magnetic field orientation, pump laser absorption in the atmosphere, detection of the wakefield signal, possibility of inducing O_2 lasing.

Acknowledgement: We would like to acknowledge Dr. S. Potashnik for useful discussions. This work was supported by the Naval Research Laboratory Base Fund.

Appendix A. Transitions in Oxygen Molecule

Oxygen's abundance in the earth's atmosphere, approximately 21 % $\left(N = 5.7\times10^{18}\,\mathrm{cm}^{-3}\right)$ and its paramagnetic response make it a possible candidate species for a remote optical magnetometer [4-7]. Molecular oxygen O_2 has two unpaired electrons in the upper level of the ground state, giving it a paramagnetic response. The ground state of oxygen $X^3\Sigma_g^-$, commonly referred to as "triplet oxygen," has total spin $S=1$ and three degenerate sublevels. In atmospheric conditions near the surface of the earth (pressure $P = 1\,\mathrm{atm}$, total number density $N_{\mathrm{air}} = 2.7\times10^{19}\,\mathrm{cm}^{-3}$, and temperature $T = 23.5\mathrm{meV}$), the ground state is fully populated because the next excited electronic state's energy, $E_a = 0.98\mathrm{eV}$ is much greater than the thermal energy.

The electronic configuration of molecular oxygen is shown in Fig. 8. The first excited electronic state of oxygen, $a^1\Delta_g$, is referred to as "singlet oxygen" and only has one spin state $(S,m)=(0,0)$. This state has an energy of $E_{\mathrm{a-X}} = 0.98\mathrm{eV}$, $a^1\Delta_g$ can undergo spontaneous emission via a magnetic dipole transition to the ground state $O_2\left(a^1\Delta_g - X^3\Sigma_g^-\right)$ or $\mathrm{a-X}$. The $\mathrm{a-X}$ transition has a wavelength of $1.27\,\mu\mathrm{m}$. This transition is dominantly due to the orbital angular momentum $\boldsymbol{L}$ and has spontaneous emission rate of $A_{\mathrm{a-X}} = 2\times10^{-4}\ \mathrm{sec}^{-1}$ [14].

The second excited state of oxygen $b^1\Sigma_g^+$ will be referred to as the upper state. It is also a spin singlet state with only one sublevel. The upper state can undergo three radiative transitions; $b^1\Sigma_g^+ - X^3\Sigma_g^-(m=\pm1)$, $b^1\Sigma_g^+ - X^3\Sigma_g^-(m=0)$ and $b^1\Sigma_g^+ - a^1\Delta_g$ where the first and second transitions are between the different magnetic sublevels of the ground state and are referred to as the A band [11]. The transitions will be referred to as $\mathrm{b-X},1$, $\mathrm{b-X},0$, and $\mathrm{b-a}$ respectively. The $\mathrm{b-X}$ transitions have an energy of $E_{\mathrm{b-X}} = 1.63\mathrm{eV}$, wavelength $\lambda_{\mathrm{b-X}} = 762\,\mathrm{nm}$, and frequency $\omega_{b-X} = 2.5\times10^{15}\,\mathrm{rad}\cdot\mathrm{sec}^{-1}$. The calculated spontaneous emission rates of the $\mathrm{b-X},1$ and $\mathrm{b-X},0$ transitions are $A_{\mathrm{b-X},1} = 0.087\mathrm{sec}^{-1}$ and $A_{\mathrm{b-X},0} = 1.6\times10^{-7}\mathrm{sec}^{-1}$ respectively [14]. The radiation from the $\mathrm{b-X},1$ transition can be seen in air-glow, night-glow and aurorae [14]. The $\mathrm{b-X},1$ transition is magnetic dipole- and spin-forbidden and it is dominant over the $\mathrm{b-a}$ and $\mathrm{b-X},0$ transitions which are electric quadrupole transitions [11]. This can be explained by a large spin-orbit coupling between the $b^1\Sigma_g^+$ state and the $X^3\Sigma_g^-(m=0)$ state. The spin-orbit coupling results in a mixing of the levels and the $\mathrm{b-X},1$. The $\mathrm{b-a}$ transition has an energy of $E_{\mathrm{b-a}} = 0.65\mathrm{eV}$, wavelength $\lambda_{\mathrm{b-a}} = 1.9\,\mu\mathrm{m}$, frequency $\omega_{b-a} = 9.9\times10^{14}\,\mathrm{rad}\cdot\mathrm{sec}^{-1}$ and spontaneous emission rate of $A_{\mathrm{b-a}} = 1.4\times10^{-4}\mathrm{sec}^{-1}$ [14]. The transitions from the upper $b^1\Sigma_g^+$ can be monitored by luminescence spectroscopy [14].

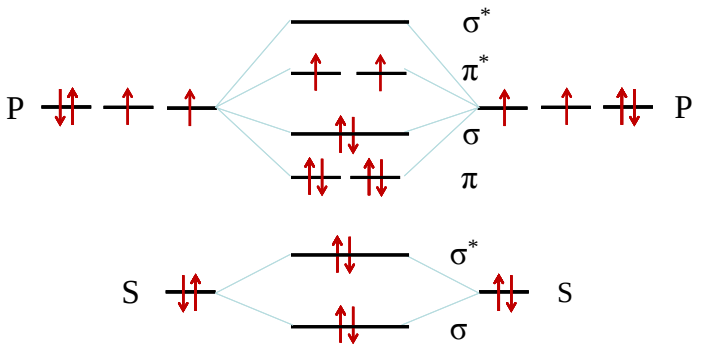

Figure 8: Electron occupancy energy levels of O_2 as two oxygen molecules are brought together.

Appendix B. Density Matrix Equations

Interaction of an oxygen molecule with radiation is governed by Schrödinger's equation $i\hbar\partial\psi/\partial t = H\psi$ where $H = H_0 - \boldsymbol{\mu}_m \cdot \boldsymbol{B}(t)$ is the full Hamiltonian, H_0 is the electronic Hamiltonian after Zeeman splitting, and $-\boldsymbol{\mu}_m \cdot \boldsymbol{B}(t)$ is the magnetic dipole interaction energy. The wavefunction $\psi(\boldsymbol{r},t) = \sum_n C_n(t) u_n(\boldsymbol{r})$ can be decomposed into the orthogonal energy eigenstates of O_2, $u_n(\boldsymbol{r})$. The probability amplitudes $C_n(t)$ are related to the density matrix elements $\rho_{nm}(t) = C_n(t) C_m^*(t)$. The macroscopic electromagnetic fields are driven by a statistical ensemble of molecules, not a single molecule, and therefore it is necessary to use the density matrix equations and to introduce phenomenological relaxations terms, i.e., $\partial\rho_{nm}/\partial t = -i\omega_{nm}\rho_{nm} + i\sum_\ell \{\Omega_{nl}\rho_{lm} - \Omega_{lm}\rho_{ln}\} + \text{relaxation terms}$.

In our model molecular oxygen is treated as a closed four level atom composed of the ground state $O_2\left(X^3\Sigma_g^-\right)$ and the upper level $O_2\left(b^1\Sigma_g^+\right)$. The ground state has three spin sublevels $m = -1, 0, +1$ which are referred to as states $|1\rangle$, $|2\rangle$, and $|3\rangle$ respectively. The excited upper level is referred to as state $|4\rangle$. The complete set of coupled equations for the density matrix elements, assuming a closed system, are given by

$$\partial\rho_{11}/\partial t = -\left(\Gamma_{12} + \Gamma_{13}\right)\rho_{11} + \Gamma_{21}\rho_{22} + \Gamma_{31}\rho_{33} + \Gamma_{41}\rho_{44} + i\left(\Omega_{14}\rho_{41} - \Omega_{41}\rho_{14}\right), \tag{B1}$$

$$\partial\rho_{22}/\partial t = \Gamma_{12}\rho_{11} - \left(\Gamma_{21} + \Gamma_{23}\right)\rho_{22} + \Gamma_{32}\rho_{33} + \Gamma_{42}\rho_{44}, \tag{B2}$$

$$\partial\rho_{33}/\partial t = \Gamma_{13}\rho_{11} + \Gamma_{23}\rho_{22} - \left(\Gamma_{31} + \Gamma_{32}\right)\rho_{33} + \Gamma_{43}\rho_{44} + i\left(\Omega_{34}\rho_{43} - \Omega_{43}\rho_{34}\right), \tag{B3}$$

$$\partial\rho_{44}/\partial t = -\left(\Gamma_{41} + \Gamma_{42} + \Gamma_{43}\right)\rho_{44} + i\left(\Omega_{41}\rho_{14} - \Omega_{14}\rho_{41}\right) + i\left(\Omega_{43}\rho_{34} - \Omega_{34}\rho_{43}\right), \tag{B4}$$

$$\partial\rho_{41}/\partial t = -\gamma_{41}\rho_{41} - i\omega_{41}\rho_{41} + i\,\Omega_{41}\left(\rho_{11} - \rho_{44}\right) + i\,\Omega_{43}\rho_{31}, \tag{B5}$$

$$\partial\rho_{43}/\partial t = -\gamma_{43}\rho_{43} - i\omega_{43}\rho_{43} + i\,\Omega_{43}\left(\rho_{33} - \rho_{44}\right) + i\,\Omega_{41}\rho_{13}, \tag{B6}$$

$$\partial\rho_{13}/\partial t = -\gamma_{13}\rho_{13} - i\omega_{13}\rho_{13} + i\,\Omega_{14}\rho_{43} - i\,\Omega_{43}\rho_{14}, \tag{B7}$$

The population level of state $|n\rangle$ is given by ρ_{nn} while the coherence between the states are given by $\rho_{nm} = \rho_{mn}^{*}$. The transition frequencies are defined as $\omega_{mn} = \omega_m - \omega_n$ where $\hbar\omega_n$ is energy of the n[th] state. For example, the state frequencies are $\omega_1 = -\Omega_o$, $\omega_2 = 0$, $\omega_3 = \Omega_o$, and $\omega_4 = \omega_A$ and the transition frequencies are $\omega_{41} = \omega_A + \Omega_o$, $\omega_{13} = -2\Omega_o$, and $\omega_{43} = \omega_A - \Omega_o$, where ω_A is $O_2\left(b^1\Sigma_g^+ - X^3\Sigma_g^-\right)$ transition frequency in the absence of a magnetic field. The Larmor frequency is given by $\Omega_o = qB_o/(2mc)$ where q is the electric charge, B_o is the static background magnetic field, and m is the electron's mass. Equations (B1)-(B7) imply conservation of population levels, i.e., $\partial(\rho_{11} + \rho_{22} + \rho_{33} + \rho_{44})/\partial t = 0$ (closed system). The populations are additionally normalized unity, i.e. $\mathrm{Tr}(\rho) = 1$. The interaction frequency between states m and state n is $\Omega_{mn} = \Omega_{nm}^{*}$. Specifically, $\hat{\Omega}_{43}(z,t) = \mu_m \hat{B}_R(z,t)/\hbar$ and $\hat{\Omega}_{41}(z,t) = \mu_m \hat{B}_L(z,t)/\hbar$ where μ_m is the effective magnetic dipole moment between triplet oxygen and the upper state and $\hat{B}_{R,L}$ corresponds to is the right, handed polarization of the pump field. The rate equation for ρ_{42} is not considered since it does not couple to the those in Eqs.(B1)-(B7).

The rates γ_{41} and γ_{43} consist of contributions from i) elastic collisions (soft, dephasing collisions with no population transfers), ii) inelastic collisions (population transferring) and spontaneous emission. The elastic collision rate is taken to be the dominate rate and we set $\gamma_{41} = \gamma_{43} = \gamma_{31} = \gamma_c$. In the absence of the pump field and at equilibrium we have $\rho_{11} = \rho_{22} = \rho_{33} = \rho_o$ and $\rho_{44} = 0$. This implies that $\Gamma_{21} = \Gamma_{12}$, $\Gamma_{31} = \Gamma_{13}$ and $\Gamma_{23} = \Gamma_{32}$ and we take these rates, which include inelastic collisions and spontaneous emission, to equal Γ_o. In addition, the rates Γ_{41}, Γ_{42} and Γ_{43} consist of inelastic collisions and spontaneous emission and we take these rates to be equal to Γ_U. Taking the inelastic collision rates to be equal, i.e. $\Gamma_o = \Gamma_U$, the density matrix equations become

$$\partial\rho_{11}/\partial t = -\gamma_o(\rho_{11}-\rho_{11}^{eq}) + i\left(\Omega_{14}\rho_{41}-\Omega_{41}\rho_{14}\right), \tag{B8}$$

$$\partial\rho_{22}/\partial t = -\gamma_o(\rho_{22}-\rho_{22}^{eq}), \tag{B9}$$

$$\partial\rho_{33}/\partial t = -\gamma_o(\rho_{33}-\rho_{33}^{eq}) + i\left(\Omega_{34}\rho_{43}-\Omega_{43}\rho_{34}\right), \tag{B10}$$

$$\partial\rho_{44}/\partial t = -\gamma_o(\rho_{44}-\rho_{44}^{eq}) + i\left(\Omega_{41}\rho_{14}-\Omega_{14}\rho_{41}\right) + i\left(\Omega_{43}\rho_{34}-\Omega_{34}\rho_{43}\right), \tag{B11}$$

$$\partial\rho_{41}/\partial t = -\gamma_c\rho_{41} - i\omega_{41}\rho_{41} + i\Omega_{41}\left(\rho_{11}-\rho_{44}\right) + i\Omega_{43}\rho_{31}, \tag{B12}$$

$$\partial\rho_{43}/\partial t = -\gamma_c\rho_{43} - i\omega_{43}\rho_{43} + i\Omega_{43}\left(\rho_{33}-\rho_{44}\right) + i\Omega_{41}\rho_{13}, \tag{B13}$$

$$\partial\rho_{13}/\partial t = -\gamma_c\rho_{13} - i\omega_{13}\rho_{13} + i\Omega_{14}\rho_{43} - i\Omega_{43}\rho_{14}. \tag{B14}$$

The phenomenological inelastic damping rate is given by $\gamma_o = 3\Gamma_o = 3\Gamma_U \approx 10^8\,\mathrm{sec}^{-1}$ [6]. The equilibrium populations for the ground state are $\rho_{11}^{eq} = \rho_{22}^{eq} = \rho_{33}^{eq} = 1/3$ and for the upper state $\rho_{44}^{eq} = 0$.

Appendix C. Resonant Fluorescent Excitation (Hanle effect)

At sufficiently high intensities laser induced fluorescence, i.e. Hanle effect, can be considered. The Hanle effect refers to the depolarization of resonant fluorescence lines by an external magnetic field [1,2,10]. It provides a sensitive experimental technique for a number of measurements, including remote measurement of planetary magnetic fields [15] and spontaneous emission rates [10], and spin depolarization rates [16]. It is also the basis of one of the most sensitive methods for measuring the lifetime of excited levels of atoms and molecules [17]. In the presence of a magnetic field the Zeeman sublevels of the ground state are split, resulting in a difference in the resonance frequencies for LHP and RHP light. The resulting phase difference between LHP and RHP light which is dependent on the ambient magnetic field, alters the polarization of fluorescing radiation.

To discuss this mechanism in more detail we consider a short intense laser pulse polarized in the x–direction $\mathbf{E}_{\mathrm{pump}} = \hat{E}_o(\tau)e^{-i\omega\tau}\ (\hat{\mathbf{e}}_R + \hat{\mathbf{e}}_L) + \mathrm{c.c.}$ This is just one of many orientations and configurations of the pump polarization and magnetic field direction in which the Hanle effect can occur.

The pump pulse is intense enough to excite level $|4\rangle$ at the expense of levels $|1\rangle$ and $|3\rangle$. The pump pulse duration τ_p is short compared to the collision time which in turn is short compared to a Larmor period. As the short duration, high-intensity polarized pump pulse sweeps

by it leaves behind an excited state which fluoresces with polarization components different then that of the pump. The fluorescence from the excited state ρ_{44} to states ρ_{11} and ρ_{33} is described by the off-diagonal coherence of the molecular density matrix elements $\rho_{43} = -i\widehat{\Omega}_{RO}\tau_p\rho_{44}e^{-i(\omega_{43}-i\gamma_c)\tau}$ and $\rho_{41} = -i\widehat{\Omega}_{LO}\tau_p\rho_{44}e^{-i(\omega_{41}-i\gamma_c)\tau}$, where $\Omega_{RO} = -i\mu_m E_o/\hbar$, $\Omega_{LO} = i\mu_m E_o/\hbar$, $\omega_{43} = \omega - \Omega_o$ and $\omega_{41} = \omega + \Omega_o$. The magnetization left behind the pump pulse is $\mathbf{M} = -M_o e^{-\gamma_c\tau}(e^{-i\omega_{43}\tau}\hat{\mathbf{e}}_R - e^{-i\omega_{41}\tau}\hat{\mathbf{e}}_L) + \text{c.c.}$ where $M_o = N\mu_m^2 (E_o/\hbar)\tau_p\rho_{44}$. The associated current density is $\mathbf{J}_M = -M_o e^{-\gamma_c\tau}\left[\omega_{43}\left\{\cos(\omega_{43}\tau) - i\sin(\omega_{43}\tau)\right\}\hat{\mathbf{e}}_R + \omega_{41}\left\{\cos(\omega_{41}\tau) - i\sin(\omega_{41}\tau)\right\}\hat{\mathbf{e}}_L\right] + \text{c.c.}$, where $\omega_{43}, \omega_{41} \gg \gamma_c$. The current density has components in the x and y directions [10] which, for $\omega \gg \Omega_o$, are given by

$$\mathbf{J}_M = -2M_o e^{-\gamma_c\tau}\omega\cos(\omega\tau)\left[\cos(\Omega_o\tau)\hat{\mathbf{e}}_x - \sin(\Omega_o\tau)\hat{\mathbf{e}}_y\right]. \qquad \text{(C1)}$$

By using polarizer filters, the time average intensity on a detector due to the x and y components of the current density can be measured separately. Taking the ratio of the intensities from the x and y components of $\mathbf{J}_M$ gives $I_x/I_y \propto \cot^2(\Omega_o\tau)$. The ratio is independent of the collision rate as long as the individual intensities are greater than the inherent intensity fluctuations.

References

[1] D. Budker, W. Gawlik, D.F. Kimball, S.M. Rochwester, V.V. Yashchuk and A. Weis, Rev. Mod. Phys. **74**, 1154 (2002).

[2] *Optical Magnetometry*, D. Budker and D.F.J. Kimball (eds.) (Cambridge U. Press, Cambridge, UK, 2013).

[3] G. Bison, R. Wynands, and A. Weis, Appl. Phys. B Lasers Opt. **76**, 325 (2003).

[4] J.P. Davis, M.B. Rankin, L.C. Bobb, C. Giranda, M.J. Squicciarini, "REMAS Source Book," Mission and Avionics Tech. Dept., Naval Air Development Center (1989).

[5] R.J. Brecha, L.M. Pedrotti and D. Krause, J. Opt. Soc. Am. B **14**, 1921 (1997).

[6] W. Happer and A.C. Tam, "Remote Laser Pumping of Molecular Oxygen in the Atmosphere for Magnetic Field Measurements," Naval Air Development Center Report N62269-77-M-4202 (1977).

[7] R. J. Brecha, Appl. Opt. **37**, 4834 (1998).

[8] P. Sprangle, J.R. Peñano and B. Hafizi, Phys. Rev. E **66**, 046418 1-21 (2002).

[9] A. Couairon and A. Mysyrowicz, Phys. Rep. **441**, 47 (2007).

[10] P.W. Milonni and J.H. Eberly, *Laser Physics* (Wiley, Hoboken, NJ, 2010).

[11] B. Minaev, O. Vahtras, and H. Ågren, Chem. Phys. **208**, 299 (1996).

[12] R.W. Boyd, *Nonlinear Optics* (Elsevier, Burlington, MA, 2008).

[13] M. Scully and S. Zubairy, *Quantum Optics* (Cambridge U. Press, Cambridge, UK, 1997).

[14] B. F. Minaev and H. Ågren, J. Chem. Soc., Faraday Transactions, **93**, 2231 (1997).

[15] C. Kumar, L. Klein, and M. Giraud, in Work. Adv. Technol. Planet. Instruments, edited by J. Appleby (Lunar and Planetary Institute, Fairfax, Virginia, 1993), p. 14.

[16] S. Curry, W. Happer, A. Tam, and T. Yabuzaki, Phys. Rev. Lett. **40**, 67 (1978).

[17] A. Corney, *Atomic and Laser Spectroscopy*, (Oxford Univ. Press, Oxford, 2006) p. 478.